RSC Advances

ROYAL SOCIETY OF CHEMISTRY

www.rsc.org/advances

TOC

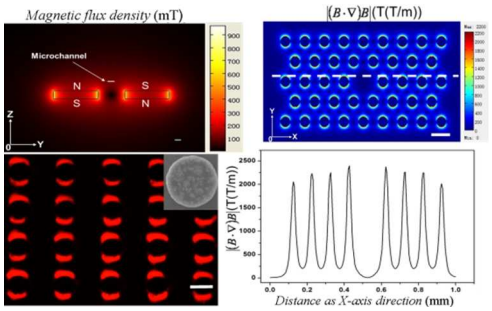

A simple and robust approach to control of the localized magnetic field distributions in microfluidic chips by nickel powder@PDMS pillars was established.

RSC Advances

RSCPublishing

ARTICLE

Control of magnetic field distribution by using nickel powder@PDMS pillars in microchannels

Cite this: DOI: 10.1039/x0xx00000x

Xu Yu,[abc] Cong -Ying Wen,[ab] Zhi-Ling Zhang [ab*] and Dai-Wen Pang [ab]

Received ooth January 2012,
Accepted ooth January 2012

DOI: 10.1039/x0xx00000x

www.rsc.org/

A simple and robust approach to control the magnetic field distribution by nickel powder@PDMS pillars was established. The nickel powder@PDMS pillars were fabricated in several simple steps, using a simple and robust method, and no training in techniques or expensive equipment is necessary comparing to other methods. The localized magnetic field distributions in the microchannels can be tailored by the nickel powder@PDMS pillars with automatically generating of high magnetic field gradients around them due to the high relative magnetic permeability of the nickel powder@PDMS. The numerical simulation and red fluorescent magnetic nanoparticle capture experiment results convinced that our approach can effectively control the localized magnetic field distribution in the microchannels. Two kinds of the tailoring events were studied by the powder@PDMS pillars in the microchannels underneath of two different external magnetic fields. To our best knowledge, it is for the first time to report that different localized magnetic field distributions were obtained in the microchannels by nickel powder@PDMS pillars due to the difference of the external magnetic fields. This approach were used to capture fluorescent magnetic nanoparticles and magnetic bead-yeast cell complexes. We believe that this approach have a great potential applications in the chemistry, biology, biomedicine and tissue engineering.

Introduction

Magnetic nanoparticles, owing to many advantages such as high magnetization values, flexible surface functionalization, simplemanipulation by magnets and good biocompatibility, were widely used in therapy, diagnosis, tissue engineering, and other biomedical applications [1, 2]. Microfluidic chip can integrate multiple functional units into one chip with strong points of reagents saving, low cost and time consuming. A strategy that combines magnetic nanoparticles and microfluidic chips can remove tremendous washing process [3, 4], enhance their advantages, and maximize their applicability [5, 6]. However, it is a big challenge to capture the magnetic nanoparticles at a high flow velocity (typically at dozens of microliters per minute) due to low magnetic field gradients in the microchannels [7, 8]. The magnetic nanoparticles captured at low flow velocities in microfluidic chips (less than 1-2 microliter per minute) was low throughput and not a good choice for many applications. Also, it was not efficient to remove waste and the non-specifically adsorptions [9] on the magnetic nanoparticles. It is important and significant to control the localized magnetic field distributions in order to capture the magnetic nanoparticles at high flow velocities. Nickel and Ni-Fe alloys were applied to increase the localized magnetic field gradients in the microchannels [10, 11], owing to their significantly higher magnetic permeability of nickel relative to the buffer solution [9, 12, 13]. In our previous study, we have used the poly(dimethylsiloxane) (PDMS) encapsulated nickel patterns to control the magnetic field distribution and pattern magnetic bead arrays for on-chip detection of the multiple cancer biomarkers [3, 14]. The nickel patterns were fabricated by electroplating process which needs electroplating instruments, electroplating bath composition, intensive labour and many waste-generations.

Here comes a new approach to tailor the localized magnetic field distribution in the microchannels by using the nickel powder@PDMS pillars was reported. The pillars were composed by most of the nano-size nickel powders and a little of PDMS. Two kinds of different localized magnetic field distributions were studied in the micrchannels at two different external magnetic fields. The red fluorescent-magnetic nanoparticles [2, 15-17] were captured in the microchannels in order to observe the local magnetic field distributions. We also used the COMSOL Multiphysics 3.5a software to simulate the localized magnetic field distributions in the microchannels. The simulation results agreed with the experiment results and convinced that our approach could effectively control the localized magnetic field distribution in the microchannels. Our approach has many advantages: (1) The localized magnetic field distribution in the microchannels could be tailored by the nickel powder@PDMS pillars. By using nickel powder@PDMS pillars, there were higher magnetic field

gradients around the nickel powder@PDMS pillars in the microchannels. (2) The nickel powder@PDMS pillars were generated in several simple steps, using a simple and robust method, and no training in electroplating techniques was necessary. (3) To the best of our knowledge, other materials which have high relative permeability such as iron powder, nano Fe_3O_4 particles or nickel iron alloy particles et al. can be used as the same purpose for control of the local magnetic field in the microchannels. (4) This approach could be used to capture magnetic nanoparticles and generate the magnetic nanoparticle arrays which could be used for cancer cell sorting, immunoassays, drug delivery, drug releasing and so on. To our best knowledge, it is for the first time to report that different localized magnetic field distributions were obtained in the microchannels by nickel powder@PDMS pillars due to the difference of the external magnetic fields.

Experimental Section

Chemical reagents

SU-8 2050 photoresists and developer were purchased from MicroChem (MicroChem Corp., USA). AZ50XT photoresists and developer AZ400K were purchased from AZ Electronic Materials (AZ Electronic Materials USA Corp, USA). Poly(dimethylsiloxane) (PDMS) and curing agent were purchased from GE (GE Toshiba Silicones Co., Ltd., Japan). Nanonickel powder (50 nm, 99.9%) was obtained from DeKeDaoKing (Bejing, China). Yeast cell (Saccharomyces cerevisiae AY, BY4742) was purchased from China Center for Type Culture Collection (Wuhan University, China). Red fluorescent magnetic nanoparticles were synthesized as our previous reports [2, 15, 17-20]. MyOne carboxylic acid magnetic beads (MyOne, 1.05 μm diameter) were obtained from Dynabeads (Invitrogen Dynal, Norway). Dextrose was obtained from JingKeHongDa Bio-Tech Co., (Beijing, China). Peptone and yeast extract were purchased from BD (Bectone, Dickinson and company, USA). *N*-Ethyl-*N*'-(3-dimethyl-aminopropyl) carbodiimide hydrochloride (EDAC), N-hydroxysulfosuccinimide sodium salt (Sulfo-NHS) and 2-(*N*-morpholino) ethane sulfonic acid hydrate (MES) were obtained from Sigma-Aldrich. Bovine serum albumin (BSA) and concanavalin A (Con A) were obtained from Biosharp. Trimethylchlorosilane (TMCS), $Na_2HPO_4{\cdot}12H_2O$, NaCl, $NaH_2PO_4{\cdot}2H_2O$, Tween 20 and NaN_3 were purchased from GuoYao (Shanghai, China). All solutions were prepared with 18.2 MΩ·cm ultrapure water obtained from a Millipore water-purification system (Millipore, USA).

Fabrication of nickel powder@PDMS pillars

The fabrication of the nickel powder@PDMS pillars and the microfluidic channel was shown in Fig. 1. The microfluidic chip with nickel powder@PDMS pillars was fabricated as the following steps. First, the standard soft lithography technology was used to fabricate the SU-8 mould. Briefly, the SU-8 2050 photoresist was spin coated on a clean silicon wafer to fabricate a ~ 40 μm SU-8 mould with 50-100 μm holes by using a designed mask of different shapes. Then the silicon SU-8 mould was exposed to TMCS vapour for 2 min in order to facilitate the mould release. Then the nickel powders (50 nm) were filled into the holes on the the silicon SU-8 mould with the aid of a small brush. Then the degassed RTV615A and RTV615B components were mixed at a ratio of 10 : 1 by weight and casted on the silicon SU-8 mould for a thickness about 500 μm and then kept in 75 ºC for 1 hour. After that, the solidified PDMS pattern was peeled off from the silicon SU-8 mould with the nickel powders. Some of the prepolydimethylsiloxane flew into the nickel powders holes and cured to form the nickel powder@PDMS pillars. The PDMS pattern with nickel powder@PDMS pillars was bound to a clean slide glass for composing the microfluidic chip (Fig. 1(A)). This method for fabrication of the nickel powder@PDMS pillars was simple and robust as well as the renew use of the silicon moulds. By designing different shape holes in the moulds, we can obtain different shaped nickel powder@PDMS pillars, which could be used for generation of different magnetic nanoparticle patterns in microfluidic chips.

Fabrication of microfluidic channels

The fluidic microchannel layer was fabricated in standard soft lithography method [21]. AZ50XT photoresist was spin coated on a silicon wafer to fabricate a about 40 μm thick positive mould. The PDMS mixture (RTV615A : RTV615B = 10 : 1 (w/w)) was poured onto the silicon mould and baked at 75 ºC for 4 hours. The solid PDMS was peeled off from the positive mould and punched with a blunt needle for inlets and outlets, as shown in Fig. 1(B). Afterwards, the microchannel layer was irreversibly bonded to the PDMS pattern with nickel powder@PDMS pillars (Fig. 1(C)).

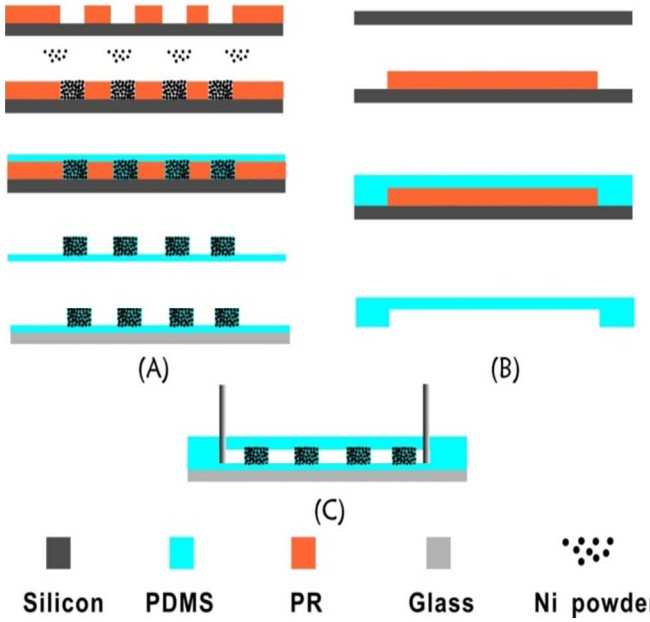

Fig. 1 Fabrication process of the microfluidic chip with integrated nickel powder@ PDMS pillars. (A) Fabrication of the nickel powder@PDMS pillars. (B) Fabrication of the microfluidic channel. (C) Side view of the integrated microfluidic chip with nickel powder@ PDMS pillars.

The external magnetic fields acting on the microfluidic chip

The localized magnetic field distribution in the microchannels were studied under two kinds of different external magnetic fields: (1)

Two permanent magnets were fixed on a glass slide to generate an "NS" pole and put under each side of the microchannel (the gap of the permanent magnets was 6 mm) for providing a relatively uniform magnetic field with the magnetic flux density about 105 mT [14]. (2) Only one permanent magnet was put under the microchannel for providing a upright magnetic field through the microchannel.

Results and Discussions

SEM and optical imaging of the nickel powder@PDMS pillar arrays

Scanning electron microscope (SEM) provided a straightforward way to characterize the nickel powder@PDMS pillars. Fig. 2 showed the SEM results of the nickel powder@PDMS pillars. There were nickel powders on the surfaces of the PDMS pillars, which demonstrated that the nickel powders were filled into holes and doped into the PDMS pillars. The optical images of the nickel powder@PDMS pillars were shown in the Electronic Supplementary Information (ESI†, Fig. S1). The optical images demonstrated that the nickel powders (black) were filled out into the PDMS pillars. Moreover, by designing different shaped holes in the photoresist mould, we can obtain the correspondingly shaped nickel powder@PDMS pillars in the microchannels. As results, a large area of regular nickel powder@PDMS pillar patterns in the microchannels without any defects can be fabricated by using this robust and simple method.

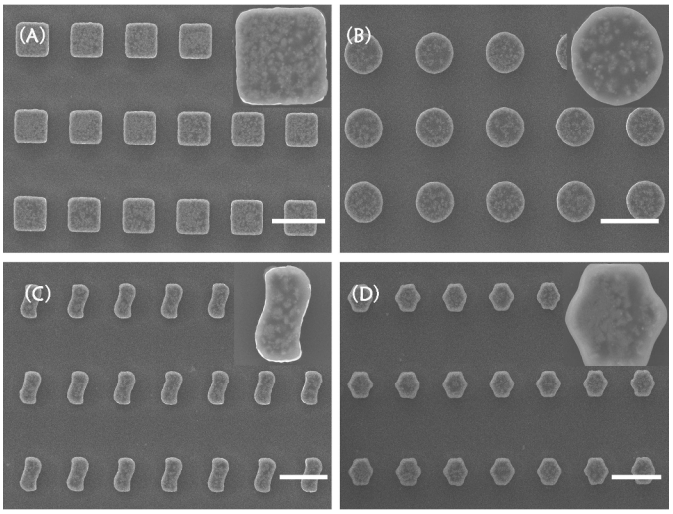

Fig. 2 SEM image of the nickel powder@PDMS pillars. (A) 90 μm square shaped nickel powder@PDMS pillars. (B) 100 μm circular shape nickel powder@ PDMS pillars. (C) 65 μm "~" shaped nickel powder@ PDMS pillars. (D) 70 μm hexagonal shaped nickel powder @PDMS pillars. Inserts were amplification of single nickel powder@PDMS pillares. The scale bars are 200 μm.

The stability of the nickel powder@PDMS pillars in microchannels

The nickel powder@PDMS pillars are very stable under high velocities, such as 50 μL/min or higher. Because the nickel powders were encapsulated in the curing elasticity PDMS, they cannot leak out from the pillars. And the nickel powder@PDMS pillars are fixed on the thin PDMS bonded to a clean glass slide. We could use a ultrasound cleaner to clean the microfluidic channels and reuse the chip. They weren't destroyed even at this extreme condition.

Simulation of the external magnetic field distribution

The magnetic field is commonly described by the magnetic flux density B, which can be calculated by the equation (1) [14, 22],

$$B = \mu_0(H + M) = \mu_0(H + \chi H) = \mu_0(1 + \chi)H = \mu_0\mu_r H \quad (1)$$

μ_0 is the permeability of a vacuum ($4\pi \times 10^{-7}$, H/m), H is the magnetic field intensity (A/m), M is the magnetic moment per unit volume (A/m), χ is the volumetric magnetic susceptibility (dimensionless), μ_r is the relative permeability (dimensionless).

For the permanent magnets, the distribution can be described as the equation (2) [3, 14],

$$B = \mu_0\mu_r H + B_r \quad (2)$$

B_r is the remnant magnetic flux density, which was one where no magnetic field was present. In our model, we assumed relative permeability of the magnets (μ_r) was 1.05 and the remnant magnetic flux density of the permanent magnets (B_r) was 1.17 T as our previous reports [3, 14]. In our researches, we have studied two kinds of the magnetic field distributions in the microchannels under two different external magnetic fields. First, two permanent magnets were put at each side with opposite poles under the microchannel. The gap between two permanent magnets was 6 mm. We called this external magnetic field as magnetic field-1. The magnetic field distribution at the magnetic field-1 was shown in the ESI† (Fig. S2(A) and 2(B)). In this situation there was almost an uniform magnetic field distribution in the microchannels and the magnetic flux density was about 105 mT [14]. From the Fig. S2(B), it was clearly shown that the direction of the external magnetic field through the microchannel was as the Y-axis direction. However, if only one magnet was put underneath the microfluidic chip such as Fig. S2(C) showed (we called it magnetic field-2), the magnetic field distribution was different from that of the magnetic field-1 in the microchannel. As Fig. S2(D) showed, the direction of the external magnetic field through the microchannel was as the Z-axis direction (the arrow direction represented the direction of the magnetic field distribution). The tailoring events of localized magnetic field distributions in the microchannels by nickel powder@PDMS pillars might be influenced by the different external magnetic fields.

Simulation of the $|(\boldsymbol{B}\cdot\boldsymbol{\nabla})\boldsymbol{B}|$ under two kinds of magnetic field

The characterization of the magnetic field on the micrometer in the microchannels is tricky by common methods. We used the numerical simulation method and magnetic beads captured experiments to demonstrated the effectively control of the magnetic field distribution in the microchannels. The magnetic force acting on a magnetic nanoparticle in magnetic field can be described as the equation (3) [5, 14],

$$F_{mag} = \frac{\Delta\chi \cdot V_m \cdot (B\cdot\nabla)\, B}{\mu_0} \quad (3)$$

$\Delta\chi$ is the difference in magnetic susceptibility between the magnetic nanoparticle and the surrounding buffer medium (dimensionless), V_m is the volume of the magnetic nanoparticle (m^3), μ_0 is the permeability of a vacuum ($4\pi \cdot 10^{-7}$, $H \cdot m^{-1}$), B and ∇B are the magnetic flux density (T) and magnetic field gradient ($T \cdot m^{-1}$). From this equation, it is easy to conclude that the magnetic force is laid on the $(B \cdot \nabla)B$, if the $\Delta\chi$ and V_m are constant. $(B \cdot \nabla)B$ can be calculated by the following equation (4) [22],

$$(B \cdot \nabla)B = \begin{pmatrix} B_x \frac{\partial B_x}{\partial x} & B_y \frac{\partial B_x}{\partial y} \\ B_x \frac{\partial B_y}{\partial x} & B_y \frac{\partial B_y}{\partial y} \end{pmatrix} \quad (4)$$

We simulated the magnetic field distributions in two different external magnetic fields (magnetic field-1 (Fig. 2(A)) and magnetic field-2 (Fig. 2(C)). The directions of the external magnetic fields acting in the microchannels were different (ESI†, Fig. S2).

In the 2D model, the absolute value of $(B \cdot \nabla)B$ could be calculated by the equation (5) [14],

$$|(B \cdot \nabla)B| = \sqrt{\left(\left(B_x \frac{\partial B_x}{\partial x}\right) + \left(B_y \frac{\partial B_x}{\partial y}\right)\right)^2 + \left(\left(B_x \frac{\partial B_y}{\partial x}\right) + \left(B_y \frac{\partial B_y}{\partial y}\right)\right)^2} \quad (5)$$

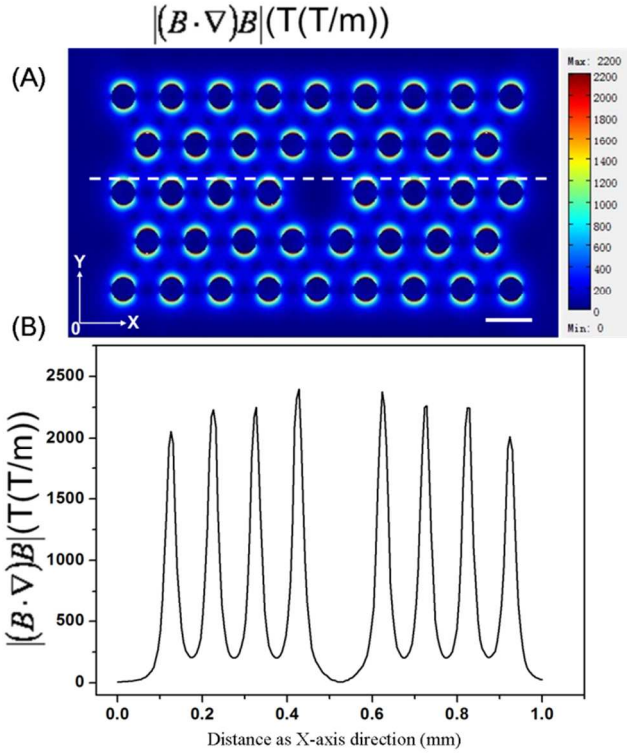

Fig. 3 The magnetic field distributions on two kinds of different external magnetic field. (A) The magnetic field distribution on two magnets composed "NS" pole (magnetic field-1). (B) The arrow display of the magnetic flux density in A (YZ-plane). (C) The magnetic field distribution on one magnet (magnetic field-2). (D) The arrow display of the magnetic flux density in C (YZ-plane). The scale bars are 1 mm.

As Fig. 3(A) showed, $|(B \cdot \nabla)B|$ had significant increase as the direction of the external magnetic field (Y-axis direction). However, in the X-axis direction, there was no obvious increase generated around the nickel powder@PDMS pillars. In the middle of the model, there was an area without the nickel powder@PDMS pillar, where no obvious increase of $|(B \cdot \nabla)B|$ along the direction of the external magnetic field-1 was found. As Fig. 3(B) shown, there were eight peaks of values of $|(B \cdot \nabla)B|$ along the X-axis direction which was corresponding to eight nickel powder@PDMS pillars. While, in the middle nickel powder@PDMS-lacked area, there was no peak value of $|(B \cdot \nabla)B|$. This demonstrated that our approach can tailor the magnetic field distribution in the microchannels by using the nickel powder@PDMS pillars

The $|(B \cdot \nabla)B|$ was simulated at the magnetic field-2 (ESI†, Fig. S3). As shown in Fig. S3, there was significant increase of the absolute value of $|(B \cdot \nabla)B|$ round the nickel powder@PDMS pillars. It also could find that high $|(B \cdot \nabla)B|$ generated around the whole areas of the nickel powder@PDMS pillars, which was different from the simulation result at the magnetic field-1 (Fig. 3). The reason was attributed to the difference of the external magnetic fields.

Control of the magnetic field distribution by nickel powder@PDMS pillars

The red fluorescent magnetic nanoparticles were applied to carry on the capture experiments in order to display the tailored magnetic field distribution by nickel powder@PDMS pillars clearly. Fig. 4(C) showed the red fluorescent magnetic nanoparticles were captured in the microchannel with nickel powder@PDMS pillars under the magnetic field-1. In this situation, the red fluorescent nanoparticles were captured at both sides around the nickel powder@PDMS pillars along the direction of the external magnetic field (Y-axis direction, Fig. S2(B)). This result agreed with the simulation results of $|(B \cdot \nabla)B|$ under the magnetic field-1 (Fig. 3). Fig. S4 also showed the red fluorescent magnetic nanoparticles were captured in the microchannel with nickel powder@PDMS pillars under the magnetic field-1. From the results, we could find that the red fluorescent magnetic nanoparticles were captured only at the areas of the pillars along the direction of external magnetic field (Y-axis direction), which was corresponding to the simulation results of $|(B \cdot \nabla)B|$ (Fig. 3) under the magnetic field-1. In addition, if there was a defect unit in the nickel powder@PDMS pillars, no red fluorescent magnetic nanoparticle was captured at the area of the defect unit, but there were red fluorescent magnetic nanoparticles captured at other areas in the same microchannels (ESI†, Fig. S5).

As Fig. 4(D) showed, there were red fluorescent magnetic nanoparticles captured around the whole cycle areas around the nickel powder@PDMS pillars under the magnetic field-2, which was also convinced by the simulation result of $|(B \cdot \nabla)B|$ at the magnetic field-2 (ESI†, Fig. S2). Moreover, we can clearly observe that no red fluorescent magnetic nanoparticle was captured in the same microchannel without nickel powder@PDMS pillar (ESI†, Fig. S6). These results demonstrated that the high magnetic field gradients automatically generated at the areas of the nickel powder@PDMS pillars, because the relative magnetic permeability of the nickel powder@PDMS ($\mu_{r(\text{nickel})} \approx 200$) was significantly larger than the relative magnetic permeability of buffer medium ($\mu_{r(\text{buffer})} \approx 1$) [9, 23]. From these results, we can deduce that high magnetic field gradients were induced in the microchannels and which were proved by the

numerical simulation results. Therefore, this simple method can be used to control the local magnetic field distribution in the microchannels.

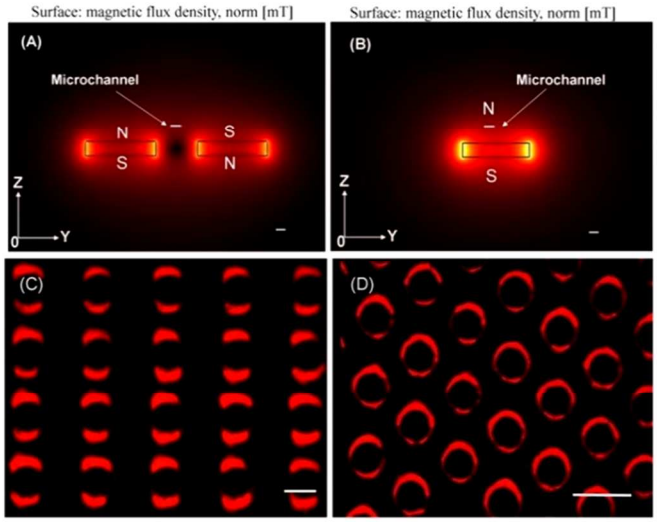

Fig. 4 (A) External magnetic field-1. (B) External magnetic field-2. (C) Fluorescence field image of the captured fluorescent magnetic beads in a microfluidic chip with opposite cylinder-shaped nickel powder@PDMS pillars under the external magnetic field-1. (D) Fluorescence field image of the captured fluorescent magnetic beads in a microfluidic chip with staggered cylinder-shaped nickel powder@PDMS pillars under the external magnetic field-2. The scale bars in (A) and (B) are 1 mm, in (C) and (D) are 100 μm.

Generation of fluorescent magnetic nanoparticle patterns

Under the controllable magnetic field, the magnetic nanoparticles could be greatly captured, thus generation of magnetic nanoparticle patterns. The magnetic nanoparticle patterns had a lot of potential applications, such as immunoassays, cell sorting, or drug releasing systems based on magnetic nanoparticles. Here we designed and fabricated two kinds of differently shaped ("~" shape and hexagon shape) nickel powder@PDMS pillars. These two nickel powder@PDMS pillars were applied to the capture of red fluorescent magnetic nanoparticles at the magnetic field-1. The results were shown in Fig. 5, which also showed that the magnetic nanoparticles were captured at the both sides of the nickel powder@PDMS pillars along the external magnetic field direction. The optical and fluorescence images of the captured red fluorescent magnetic nanoparticles also proved that our method could tailor the localized magnetic field distribution by a simple process.

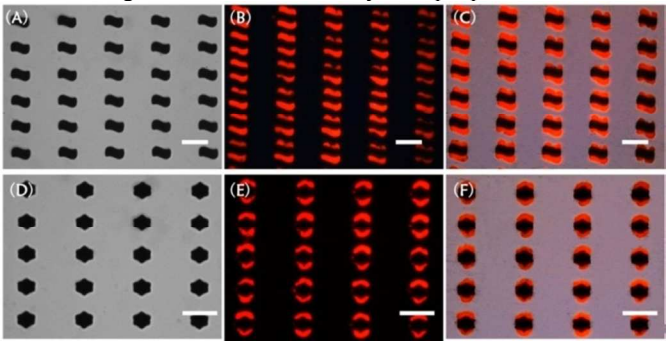

Fig. 5 Capture of red fluorescence magnetic beads in a microfluidic chip with different shaped nickel powder@PDMS pillars (magnetic field-1). (A), (D) Bright field image of "~" shaped or hexagon nickel powder@PDMS pillars. (B), (E) Fluorescence image of the captured fluorescent magnetic beads in chips with "~" shaped or hexagon-shaped nickel powder@ PDMS pillars. (C), (F) Merge of the optical image and fluorescence images of the captured fluorescent magnetic beads in the chip with "~" shaped or hexagon nickel powder@PDMS pillars. The scale bars are 100 μm.

Capture of magnetic beads-yeast cell complexes and generation of yeast cell arrays

Con A was a kind of protein, assigned to a lectin family, which was obtained from jackbean and Canavalia ensiformis [24]. And it can highly specificied and affinity reacted with carbohydrates, especially for α-D-mannosyl and α-D-glucosyl groups [24, 25], which were abundantly existed in the cell envelope of the saccharomyces cerevisiae [24,26]. In this research, the Con A modified magnetic beads were used to capture the yeasts in the magnetic field controllable microfluidic chip, generating yeast cell arrays. Fig. 6a showed a two steps coupling process of conjugating the Con A to the surfaces of the magnetic beads by using the EDC and Sulfo-NHS. The detailed process of conjugating Con A to the magnetic beads and yeast cell culture were shown in Supplementary Information. The prepared yeast cells were re-suspended in a 1.5 mL centrifuge tube and mixed with the Con A modified magnetic beads for 30 min at the room temperature with a slow rotation of 150 rpm. After generating of the yeast cell-magnetic beads complexes (Fig. 6b(A)), the mixed sample was through the magnetic field controllable microfluidic chip with nickel powder@PDMS pillars for cell sorting and the unbound yeast cells were washed out of the microfluidic chip by 1 × PBS (pH 7.4).

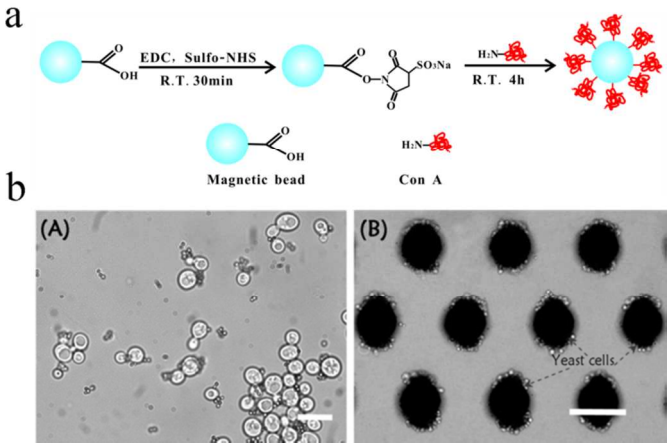

Fig. 6 a. Modification of the carboxyl magnetic beads with Con A. b. (A) Yeast cells were decorated with the Con A modified magnetic beads. (B) The yeast-magnetic bead complexes were captured at the areas around the nickel powder@PDMS pillars in a microfluidic chip. The scale bar in (A) is 10 μm and in (B) is 50 μm.

Fig. 6b(B) was the yeast cell-magnetic beads complexes were captured in the microfluidic chip with nickel powder@PDMS pillars at the magnetic field-1. It is obvious that the yeast cell-magnetic beads complexes were only captured around the nickel powder at both side areas along the direction of the external magnetic field. This yeast cell-magnetic beads arrays

could be useful for the toxicity screening system for environment [27]. In addition, this is only a model of proving that our approach could be used for cell capture and selection. We believe that this simple and robust method has great potential applications such as circulating tumour cells (CTCs) enrichment or drug releasing systems in microfluidic chips.

Conclusions

In this paper, we reported a simple and robust approach to control the magnetic field distribution by using nickel powder@PDMS pillars in the microchannels. The numerical simulation method and red fluorescent magnetic nanoparticles capture experiments were used to study the magnetic field distribution under two kinds of different external magnetic fields. These results were matched well and proved the validity of this method. In addition, the yeast cell-magnetic beads complexes were captured around the nickel powder@PDMS pillars in this magnetic field controllable microfluidic chip. We believe that this approach has great potential in practical applications in cell sorting, immunoassay or drug releasing system in microfluidics.

Acknowledgements

This work was supported by the National Basic Research Program of China (973Program, 2011CB933600), the 863 program (2013AA032204), the National Natural Science Foundation of China (21175100), and the Program for New Century Excellent Talents in University (NCET-10-0656).

Notes and references

[a]Key Laboratory of Analytical Chemistry for Biology and Medicine (Ministry of Education), College of Chemistry and Molecular Sciences, and State Key Laboratory of Virology, Wuhan University, Wuhan, 430072, P. R. China;
[b]Wuhan Institute of Biotechnology, Wuhan, 430075, P. R. China;
[c]Department of Bioengineering, Pennsylvania State University, University Park, PA 16802, USA.
*Correspondence: Professor Zhi-Ling Zhang; E-mail: *zlzhang@whu.edu.cn*; Phone: +86-27-68756759; Fax: +86-27-68754067.

Electronic Supplementary Information (ESI†) available: Culture of yeast cells. Conjugating Con A to the magnetic beads. Optical imaging of the nickel powder@pillar arrays. Simulation of the magnetic field distribution in the microchannels under the magnetic field-1 and magnetic field-2. Numerical Simulation of the $|(B\cdot\nabla)B|$under Magnetic Field-2. Control of the Magnetic Field Distribution by Nickel Powder@PDMS Pillars. See DOI: 10.1039/b000000x/

1. L. H. Reddy, J. L. Arias, J. Nicolas and P. Couvreur, *Chem Rev*, 2012, **112**, 5818-5878.
2. E. Q. Song, J. Hu, C. Y. Wen, Z. Q. Tian, X. Yu, Z. L. Zhang, Y. B. Shi and D. W. Pang, *ACS Nano*, 2011, **5**, 761-770.
3. X. Yu, H. S. Xia, Z. D. Sun, Y. Lin, K. Wang, J. Yu, H. Tang, D. W. Pang and Z. L. Zhang, *Biosens Bioelectron*, 2013, **41**, 129-136.
4. Y. H. Tennico, D. Hutanu, M. T. Koesdjojo, C. M. Bartel and V. T. Remcho, *Anal Chem*, 2010, **82**, 5591-5597.
5. N. Pamme, *Lab chip*, 2006, **6**, 24-38.
6. M. A. M. Gijs, F. Lacharme and U. Lehmann, *Chem Rev*, 2010, **110**, 1518-1563.
7. Y. J. Liu, S. S. Guo, Z. L. Zhang, W. H. Huang, D. M. Baigl, Y. Chen and D. W. Pang, *J. Appl. Phys.*, 2007, **102**, 084911.
8. R. Q. Zhang, S. L. Liu, W. Zhao, W. P. Zhang, X. Yu, Y. Li, A. J. Li, D. W. Pang and Z. L. Zhang, *Anal Chem*, 2013, **85**, 2645-2651.
9. A. Csordas, A. E. Gerdon, J. D. Adams, J. R. Qian, S. S. Oh, Y. Xiao and H. T. Soh, *Angew Chem Int Ed*, 2010, **49**, 355-358.
10. T. Deng, M. Prentiss and G. M. Whitesides, *Appl Phys Lett*, 2002, **80**, 461-463.
11. Y. J. Liu, S. S. Guo, Z. L. Zhang, W. H. Huang, D. Baigl, M. Xie, Y. Chen and D. W. Pang, *Electrophoresis*, 2007, **28**, 4713-4722.
12. J. D. Adams, U. Kim and H. T. Soh, *Proc Natl Acad Sci U S A*, 2008, **105**, 18165-18170.
13. Y. L. Liu, J. D. Adams, K. Turner, F. V. Cochran, S. S. Gambhir and H. T. Soh, *Lab chip*, 2009, **9**, 3604-3604.
14. X. Yu, X. Feng, J. Hu, Z. L. Zhang and D. W. Pang, *Langmuir*, 2011, **27**, 5147-5156.
15. J. Hu, M. Xie, C. Y. Wen, Z. L. Zhang, H. Y. Xie, A. A. Liu, Y. Y. Chen, S. M. Zhou and D. W. Pang, *Biomaterials*, 2011, **32**, 1177-1184.
16. H. Y. Xie, M. Xie, Z. L. Zhang, Y. M. Long, X. Liu, M. L. Tang, D. W. Pang, Z. Tan, C. Dickinson and W. Zhou, *Bioconjug Chem*, 2007, **18**, 1749-1755.
17. H. Y. Xie, C. Zuo, Y. Liu, Z. L. Zhang, D. W. Pang, X. L. Li, J. P. Gong, C. Dickinson and W. Z. Zhou, *Small*, 2005, **1**, 506-509.
18. L. L. Huang, P. Zhou, H. Z. Wang, R. Zhang, J. Hao, H. Y. Xie and Z. K. He, *Chem Commun*, 2012, **48**, 2424-2426.
19. G. P. Wang, E. Q. Song, H. Y. Xie, Z. L. Zhang, Z. Q. Tian, C. Zuo, D. W. Pang, D. C. Wu and Y. B. Shi, *Chem Commun*, 2005, 4276-4278.
20. E. Q. Song, G. P. Wang, H. Y. Xie, Z. L. Zhang, J. Hu, J. Peng, D. C. Wu, Y. B. Shi and D. W. Pang, *Clin Chem*, 2007, **53**, 2177-2185.
21. D. C. Duffy, J. C. McDonald, O. J. A. Schueller and G. M. Whitesides, *Anal Chem*, 1998, **70**, 4974-4984.
22. A. L. Gassner, M. Abonnenc, H. X. Chen, J. Morandini, J. Josserand, J. S. Rossier, J. M. Busnel and H. H. Girault, *Lab chip*, 2009, **9**, 2356-2363.
23. J. R. Qian, X. H. Lou, Y. T. Zhang, Y. Xiao and H. T. Soh, *Anal Chem*, 2009, **81**, 5490-5495.
24. M. Donolato, A. Torti, N. Kostesha, M. Deryabina, E. Sogne, P. Vavassori, M. F. Hansen and R. Bertacco, *Lab chip*, 2011, **11**, 2976-2983.
25. A. Touhami, B. Hoffmann, A. Vasella, F. A. Denis and Y. F. Dufrene, *Microbiology*, 2003, **149**, 2873-2878.
26. R. C. Montijn, J. van Rinsum, F. A. van Schagen and F. M. Klis, *J Biol Chem*, 1994, **269**, 19338-19342.
27. J. Garcia-Alonso, R. F. Fakhrullin, V. N. Paunov, Z. Shen, J. D. Hardege, N. Pamme, S. J. Haswell and G. M. Greenway, *Anal Bioanal Chem*, 2011, **400**, 1009-1013.

